AMERICAN SOCIETY FOR MICROBIOLOGY | Journal of Virology®

STRUCTURE AND ASSEMBLY

Antiangiogenic Vascular Endothelial Growth Factor-Blocking Peptides Displayed on the Capsid of an Infectious Oncolytic Parvovirus: Assembly and Immune Interactions

Esther Grueso,[a*] Cristina Sánchez-Martínez,[a*] Tania Calvo-López,[a] Fernando J. de Miguel,[a*] Noelia Blanco-Menéndez,[a*] Marian Fernandez-Estevez,[a*] Maria Elizalde,[a*] Jorge Sanchez,[a] Omar Kourani,[a*] Diana Martin,[a*] Aroa Tato,[a] Milagros Guerra,[a] Germán Andrés,[a] José M. Almendral[a]

[a]Centro de Biología Molecular Severo Ochoa (CSIC-UAM), Madrid, Spain

ABSTRACT As many tumor cells synthetize vascular endothelial growth factors (VEGF) that promote neo-vascularization and metastasis, frontline cancer therapies often administer anti-VEGF (α-VEGF) antibodies. To target the oncolytic parvovirus minute virus of mice (MVM) to the tumor vasculature, we studied the functional tolerance, evasion of neutralization, and induction of α-VEGF antibodies of chimeric viruses in which the footprint of a neutralizing monoclonal antibody within the 3-fold capsid spike was replaced by VEGF-blocking peptides: P6L (PQPRPL) and A7R (ATWLPPR). Both peptides allowed viral genome replication and nuclear translocation of chimeric capsid subunits. MVM-P6L efficiently propagated in culture, exposing the heterologous peptide on the capsid surface, and evaded neutralization by the anti-spike monoclonal antibody. In contrast, MVM-A7R yielded low infectious titers and was poorly recognized by an α-A7R monoclonal antibody. MVM-A7R showed a deficient assembly pattern, suggesting that A7R impaired a transitional configuration that the subunits must undergo in the 3-fold axis to close up the capsid shell. The MVM-A7R chimeric virus consistently evolved in culture into a mutant carrying the P6Q amino acid substitution within the A7R sequence, which restored normal capsid assembly and infectivity. Consistent with this finding, anti-native VEGF antibodies were induced in mice by a single injection of MVM-A7R empty capsids, but not by MVM-A7R virions. This fundamental study provides insights to endow an infectious parvovirus with immune antineovascularization and evasion capacities by replacing an antibody footprint in the capsid 3-fold axis with VEGF-blocking peptides, and it also illustrates the evolutionary capacity of single-stranded DNA (ssDNA) viruses to overcome engineered capsid structural restrictions.

IMPORTANCE Targeting the VEGF signaling required for neovascularization by vaccination with chimeric capsids of oncolytic viruses may boost therapy for solid tumors. VEGF-blocking peptides (VEbp) engineered in the capsid 3-fold axis endowed the infectious parvovirus MVM with the ability to induce α-VEGF antibodies without adjuvant and to evade neutralization by MVM-specific antibodies. However, these properties may be compromised by structural restraints that the capsid imposes on the peptide configuration and by misassembly caused by the heterologous peptides. Significantly, chimeric MVM-VEbp resolved the structural restrictions by selecting mutations within the engineered peptides that restored efficient capsid assembly. These data show the promise of antineovascularization vaccines using chimeric VEbp-icosahedral capsids of oncolytic viruses but also raise safety concerns regarding the genetic stability of manipulated infectious parvoviruses in cancer and gene therapies.

KEYWORDS VEGF, VEGF peptides, antibody footprint, capsid assembly, capsid engineering, immune evasion, infectious chimeras, parvovirus, tumor vascularization, virus evolution

Citation Grueso E, Sánchez-Martínez C, Calvo-López T, de Miguel FJ, Blanco-Menéndez N, Fernandez-Estevez M, Elizalde M, Sanchez J, Kourani O, Martin D, Tato A, Guerra M, Andrés G, Almendral JM. 2019. Antiangiogenic vascular endothelial growth factor-blocking peptides displayed on the capsid of an infectious oncolytic parvovirus: assembly and immune interactions. J Virol 93:e00798-19. https://doi.org/10.1128/JVI.00798-19.

Editor Joanna L. Shisler, University of Illinois at Urbana Champaign

Address correspondence to José M. Almendral, jmalmendral@cbm.csic.es.

* Present address: Esther Grueso and Cristina Sánchez-Martínez, Biosciences Research Institute. School of Experimental Sciences, Universidad Francisco de Vitoria, Madrid, Spain; Fernando J. de Miguel, Yale Cancer Center, Yale University School of Medicine, New Haven, Connecticut, USA; Noelia Blanco-Menéndez, Instituto de Investigación Biomédica de a Coruña (CHUAC-UDC), a Coruña, Spain; Marian Fernandez-Estevez, Cambridge Institute for Medical Research, Cambridge University, Cambridge, United Kingdom; Maria Elizalde, Center for Applied Medical Research (CIMA), University of Navarra, Pamplona, Spain; Omar Kourani, Department of Cancer Biology, Instituto de Investigaciones Biomédicas Alberto Sols (CSIC-UAM), Madrid, Spain; Diana Martin, Animal Health Research Center (CISA-INIA), Madrid, Spain.

E.G., C.S.-M., and T.C.-L. contributed equally to this work.

Received 10 May 2019
Accepted 10 July 2019
Accepted manuscript posted online 17 July 2019
Published 12 September 2019

Many tumor cells synthetize vascular endothelial growth factors (VEGF) that promote the formation of new blood vessels (angiogenesis) that favor tumor growth and metastasis (1, 2). VEGF signals mainly through two receptor tyrosine kinases, VEGF-R1 (Flt-1) and VEGF-R2 (Flk-1/KDR), the latter being the primary mediator of VEGF angiogenic activity, in association with neuropilin-1 (3). Therefore, many cancer therapies target VEGF signaling, which may not only inhibit tumor growth but also reverse the immunosuppressive state in cancer patients by indirect mechanisms (4, 5). One successful therapy is administration of the anti-VEGF (α-VEGF) neutralizing monoclonal antibody (MAb) bevacizumab (Avastin) (6), which showed clinical benefit in different tumor types (7, 8). Methods to improve this passive immunotherapy, such as the induction of polyclonal α-VEGF neutralizing antibodies by vaccination against peptides covering the bevacizumab binding site (9), are strategies under investigation. It should be mentioned, though, that the biosafety of prolonged anti-VEGF immune therapy is controversial, as systemic delivery of anti-VEGF antibodies in mice produced adverse effects in healthy vasculature (10), in contrast to the minor adverse effects observed in patients subjected to a long-term VEGF-based cancer therapeutic vaccine (11). Other peptides that also inhibit VEGF signaling and induce antiangiogenic and tumor growth inhibition (12) may reinforce this area of research. Among peptides with the capacity to block VEGF functions, the heptapeptide A7R (also named V1 [ATWLPPR]) was identified by screening a phage library against an α-VEGF antibody (13). A7R binds neuropilin-1, inhibiting VEGF binding to the VEGF-R2 receptor, and it inhibited vascular density and tumor growth (14). The peptide P6L (PQPRPL) was selected to specifically bind VEGF-R1 and neuropilin-1 after biopanning a phage display library (15). It is noteworthy that combined therapies that target VEGF-R1 and neurophilin-1 have additive effects in reducing tumor growth (16).

Current nonconventional cancer therapies also include oncolytic viruses used in multiple ongoing experimental approaches and clinical trials (17, 18). Some members of the *Parvoviridae* (19) are among the viruses being developed as oncolytic agents on the basis of their preference for infection of human transformed cells and their lytic capacity (20–22). Adeno-associated virus (AAV) and parvovirus H-1 (H-1PV) are undergoing clinical trials in cancer patients (22, 23), and minute virus of mice (MVM), a mouse pathogen (24, 25) that lacks pathogenicity for humans, is also being tested as an oncolytic agent because of its acute lytic effects on diverse human tumor types (26–30) and anticancer effect in animal models (31). Parvoviruses and other oncolytic viruses targeting the tumor vasculature are being developed through a variety of approaches pursuing indirect antitumor effects. For example, VEGF/VEGF-R2 signaling sensitizes endothelial cells to oncolytic vaccinia virus (32), many adenoviruses have been armed to suppress VEGF and other angiogenic factors (33, 34), and the bevacizumab antibody has been expressed from AAV vectors to suppress ovarian cancer growth and metastatic lung tumors (35, 36). However, to our knowledge, no infectious oncolytic virus has been genetically engineered to structurally display antiangiogenic VEGF-blocking peptides (VEbp). Such chimeric viruses, in addition to their inherent direct antitumor effects, could induce anti-VEGF immune responses with improved clinical benefits over current passive therapies.

The parvovirus capsid is a powerful antigen-presenting vehicle that elicits long-lasting humoral and cellular immunity without adjuvant against inserted heterologous peptides (37–40). However, the tight structural organization of small icosahedral particles imposes severe engineering restrictions when the functions of the inserted peptides, as well as virus infectivity, must both be preserved. The parvovirus capsid has been extensively manipulated with heterologous peptides for multiple immune applications and retargeting purposes (41–47), although the causes of common failures of infectivity were generally not mechanistically determined. Insertions of heterologous peptides even at the most exposed loops may hamper virus-like-particle (VLP) assembly (48), but prominent loops of empty capsids and VLPs may be tolerant of the insertion of certain peptides (38, 49). However, empty capsids and VLPs markedly differed from mature DNA-filled parvovirus in both composition and posttranslational modifications

of the coat protein subunits (VPs) (50). Moreover, they do not recapitulate the multiple functions that the infectious capsid undertakes during the virus cycle, such as the cellular compartment of assembly (28) or intracellular trafficking to the nucleus for genome delivery (51).

In a previous study, we showed that insertion of the antiangiogenic A7R peptide within the flexible VPs' N-terminal domains yielded assembled noninfectious DNA-filled MVM particles, due to the failure of a VP2-Nt cleavage required to initiate infection (52). These findings prompted us to search for another capsid domain with different functional requirements and to assess substitutions of viral peptides instead of insertions into the MVM structure. The atomic structure of the MVM capsid (53, 54) showed the VP1 (83-kDa) and VP2 (64-kDa) protein subunits adopting a conformation in the β-barrel constituting eight β-sheets, with large loops interposed between the sheets, which configure the topology of the surface (Fig. 1A). As in related parvoviruses (55–57), four loops from the three subunits intertwined at the 3-fold-symmetry axis to form the spike of the capsid (22 Å long and 70 Å wide). The structure of the MVM capsid in complex with the B7-MAb neutralizing monoclonal antibody determined at 7-Å resolution by cryo-electron microscopy (cryo-EM) (58) identified a conformational epitope on the spike engaging the three symmetry-related subunits. Some of the residues involved in the MVM-B7 contacts were mutated in B7-MAb-resistant viruses isolated in mice (59). These B7-MAb-resistant mutants maintained tropism and pathogenicity, consistent with the MVM tropism determinants that mapped to a depression on the capsid 2-fold axis (60–62). These studies identified the spike as an immunodominant domain potentially suitable for the manipulation of the MVM capsid without compromising infectivity.

In the present work, the neutralizing B7-MAb epitope on the MVM capsid surface was replaced with two antiangiogenic VEbp, the VEGF mimic A7R and P6L peptides. This strategy aimed to produce chimeric parvoviruses to serve as (i) platforms for VEbp to develop antineovascularization vaccines inducing polyclonal antibodies and lasting immunity that may improve current passive tumor immunotherapy regimes, (ii) oncolytic infectious agents to combat the α-VEGF antibody resistance observed in some tumors, and (iii) infectious antigen vehicles capable of evading preexisting humoral immunity. Functions of the chimeric VEbp capsids were analyzed during the virus infection cycle and evasion of neutralizing antibodies, and the inserted peptides were studied for their surface exposure, immunogenicity, and genetic stability in prolonged cultures.

RESULTS

Chimeric MVM-VEbp engineered at the spike of the capsid. We rationally designed MVM chimeras by genetic engineering within the footprint of a neutralizing antibody resolved by cryo-electron microscopy on the 3-fold axis of the capsid (58). This epitope is formed by three intertwined subunits (54, 55) that tolerated the emergence of virus escape mutants (59). The 433-NPIGTKN-439 residues (VP2 numbering) in the three symmetry-related protein subunits that compose loop 4, are exposed on the capsid surface (Fig. 1A), and delineate the protruding B7-MAb neutralizing epitope (Fig. 1B) were replaced by either of two antiangiogenic VEbp (A7R and P6L) (Fig. 1C). The resulting chimeric viruses (MVM-A7R and MVM-P6L) were constructed in an infectious molecular clone of the prototype (p) strain of MVM (MVMp) (63), and plasmids and virus stocks were confirmed by sequencing (see Materials and Methods).

Impact of heterologous VEbp on the MVM life cycle. To analyze the effects of VEbp on the viral infectious cycle, we first studied the capacities of the MVM-VEbp chimeras for productive infection in culture. Chimeric (pMVM-P6L and pMVM-A7R) and wild-type (wt) (pMVMp) genomic clones were transfected into permissive NB324K transformed fibroblasts, and the cultures were monitored for VP expression over time (Fig. 2A). The wt transfections produced virus that rapidly spread in culture, yielding close to 100% VP-positive (VP^+) cells and patent cytopathic effect (CPE) by 120 h posttransfection (hpt). pMVM-P6L yielded similar albeit slower kinetics of cell infection

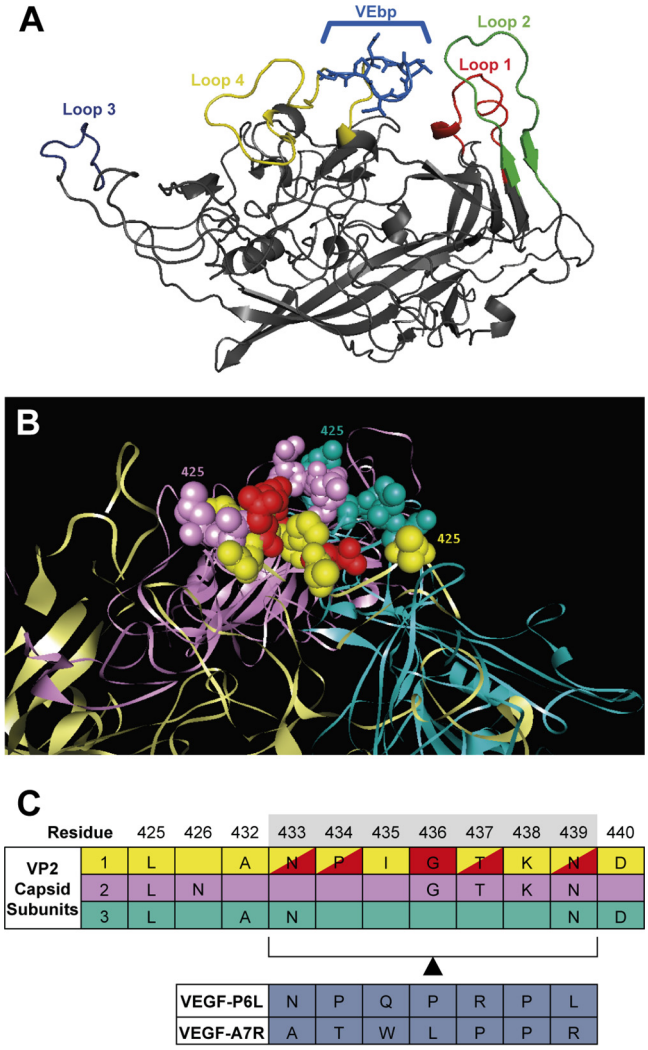

FIG 1 Engineering the MVM capsid spike with VEbp. (A) Structure of the VP2 subunit assembled in the MVMp capsid (54) showing loop 1 (red), loop 2 (green), loop 3 (dark blue), and loop 4 (yellow). The peptide within loop 4 replaced by the heterologous VEbp in chimeric viruses is shown in light blue and stick representation. (B) Configuration of the loop 4 residues replaced by VEbp. The color code and representations are as follows: balls, residues stablishing contacts with the B7-MAb (58); yellow, light blue, and pink, residues of each of the three subunits forming the spike of the capsid; and red, residues selected in MAR mutants (59) (illustrated in only one subunit). (C) Distribution of the amino acid residues in loop 4 of the three VP2 protein subunits forming the spike. Residues replaced by the VEbp are indicated (bottom). The color code is as in panel B, except that residues labeled in yellow and red are those in contact with the B7-MAb, as well as selected in MAR mutants. The software used was PyMol. The Protein Data Bank (PDB) accession number for VP2 of MVMp is 1z14 (see Movie S1 in the supplemental material).

and CPE. Although pMVM-A7R cultures showed comparable percentages of VP^+ cells at 48 hpt, no significant progression of the infection was demonstrated even at late times posttransfection.

We next investigated whether the low yield of MVM-A7R could be due to an A7R sequence-mediated impairment of viral DNA replication. For this, low-molecular-weight DNA was isolated from NB324K cells transfected by the viral genomic clones and subjected to Southern blot analysis. As shown in Fig. 2B, wt and chimeric plasmids induced correct synthesis of viral intermediate replicative forms (RF-I and RF-II). Interestingly, the single-stranded DNA (ssDNA) species associated with genome packaging into maturing viral capsids (64) were resolved only in pMVMp- and pMVM-P6L-transfected cells. This experiment demonstrated that A7R impairs the yield of packaged viral genomes.

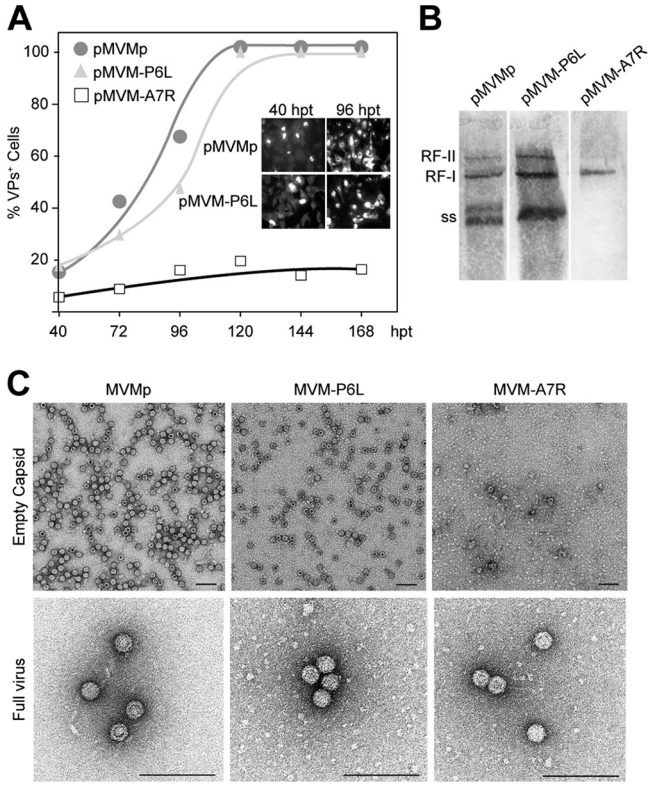

FIG 2 VEbp differentially impact the MVM infection cycle. (A) Progression of MVMp, MVM-P6L, and MVM-A7R infections in culture. Shown are the percentages of NB324K cells expressing capsid proteins (VPs) at the indicated times posttransfection by the genomic plasmids. (Inset) VP immunostaining for the wt and the pMVM-P6L plasmid. Shown is a representative experiment from three independent assays with similar outcomes. (B) MVMp, MVM-P6L, and MVM-A7R genome replication. Shown is Southern blot hybridization to low-molecular-weight DNA obtained at 48 hpt from 10^6 NB324K cells transfected by the indicated genomic plasmids. RF-I and RF-II, replicative intermediates; ss, single-stranded virus genomes. (C) EM analysis of purified empty and DNA-filled wt and VEbp chimeric viral particles. The images show representative fields from several purifications. The MVM-A7R full virus image is from a highly concentrated preparation. Scale bars, 100 nm.

The production of viral particles was determined after large-scale transfection (52) by each of the three infectious clones at 48 hpt, with yields of purified empty and DNA-filled capsids from equivalent numbers of transfected cells inspected by EM (Fig. 2C). Similar amounts of empty capsids and DNA-filled viruses were obtained from the pMVMp and pMVM-P6L transfections, with particles showing the characteristic parvoviral 25-nm diameter and morphology at high resolution. In the pMVM-A7R transfections, however, the recovery of viral particles was much lower, and fractions from CsCl gradients corresponding to the density of protein showed some MVM-A7R empty capsids and large amounts of nonparticulate aggregates. DNA-filled viruses were not detected in preliminary EM inspection of the fractions corresponding to ssDNA virus density, but they could be demonstrated at normal size and morphology upon concentration by centrifugation (Fig. 2C, bottom right).

Chimeric MVM displays VEbp on the capsid surface. The exposure and configuration of the heterologous VEbp were studied by their capacity to interact with specific antibodies in cells and *in vitro*. First, NB324K cells transfected with the wt and chimeric genomic clones were analyzed for the expression and subcellular localization of the VP viral structural proteins (Fig. 3A). Immunofluorescence (IF) staining with α-MVM capsid polyclonal antiserum showed the chimeric proteins accumulated in the nucleus at an efficiency comparable to that of the wt, indicating that the VEbp did not impair VP nuclear translocation. B7-MAb labeled the MVMp nuclear capsid formation as described previously (65), whereas it failed to recognize chimeric viral particles, consistent with

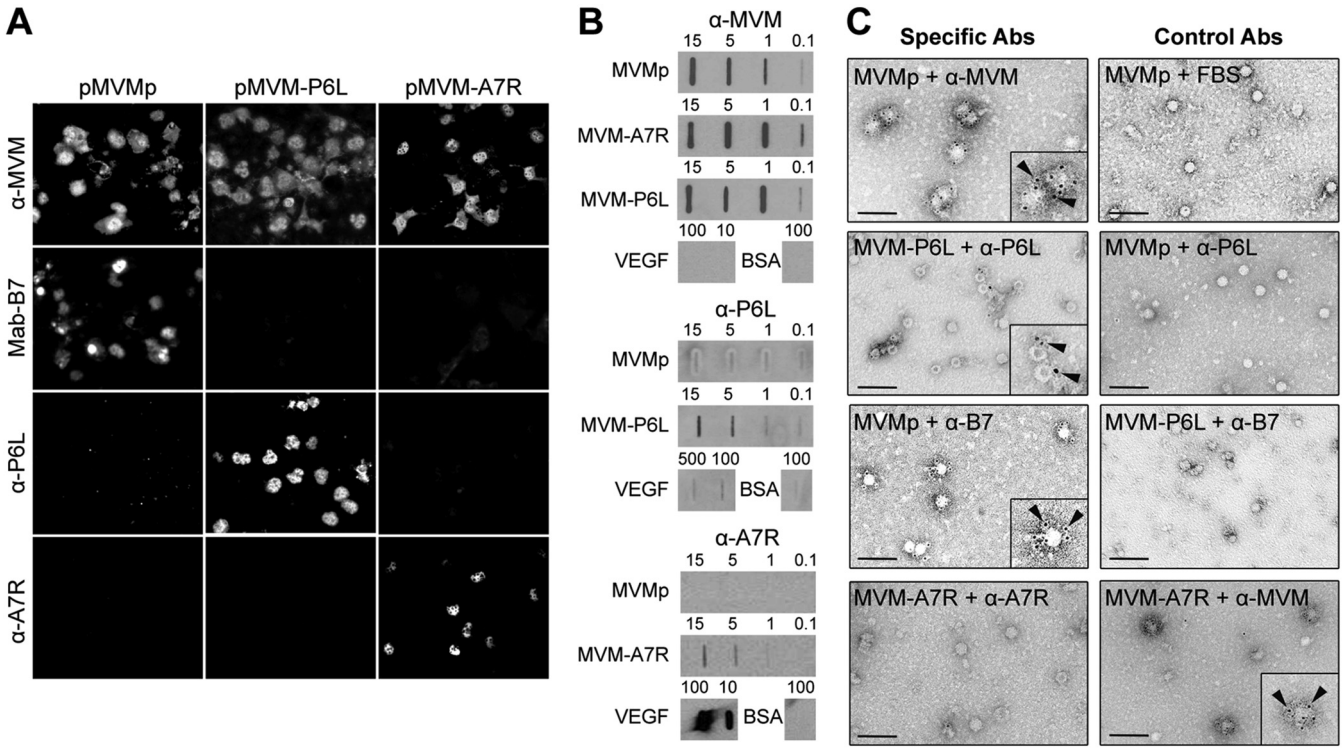

FIG 3 Antibody recognition of the VEbp displayed on chimeric capsid surfaces. (A) Confocal IF of wt and chimeric VP protein expression and subcellular localization in transfected cells. Representative stainings with the indicated α-MVM capsid, anti-3-fold wt epitope (B7-MAb), and α-VEbp specific antibodies are shown. The pMVM-A7R images showing α-MVM and α-A7R staining show the same field of cells. (B) Slot-blot analysis of VEbp surface exposure on purified viral particles. Serial dilutions of purified virions or marker proteins were applied to nitrocellulose membranes in PBS and incubated with the indicated antibodies. Virion and protein amounts (in nanograms) are shown. (C) Immunogold labeling of chimeric MVM virions bearing VEbp. Shown are representative EM fields of purified virions stained with the indicated antibodies, followed by the addition of protein A or anti-mouse IgG conjugated to 5-nm gold particles. The antibody dilutions used were 1:5 for α-MVM capsid, 1:25 for B7-MAb, and 1:2 for the α-P6L and α-A7R peptide antibodies. (Insets) The arrowheads indicate gold particles decorating viral particles. Scale bars, 100 nm.

the genetic replacement of the B7 epitope (Fig. 1). The α-P6L polyclonal antibody recognized the VP subunits in the pMVM-P6L transfections without significant signals in the wt- and VPs-A7R-expressing cells. The recognition of VP-A7R subunits by the α-A7R monoclonal antibody was significant and also specific, although the staining was detected in only a few VP-expressing cells using a high antibody concentration (Fig. 3A, bottom right).

We next addressed the exposure of the VEbp on the surfaces of purified DNA-filled virions. It should be emphasized that wt and MVM-P6L virions could be purified in sufficient amounts from cultures at 4 dpt after large-scale transfection, but obtaining similar amounts of chimeric MVM-A7R virions for the analyses required subculturing of transfected cells for 2 weeks. Virions bound to nitrocellulose filters under native conditions were first analyzed (Fig. 3B), showing that wt and both chimeric viruses maintained conformational epitopes allowing similar recognition by the anti-MVM capsid polyclonal antiserum. Both VEbp were specifically detected by the corresponding antibodies, though the signal for detection of A7R was weaker. Native VEGF was barely recognized by the α-P6L antibody but intensively by the α-A7R antibody, in agreement with the distinct methodologies used to select these VEbp peptides (13, 15). To avoid misinterpretation of peptide exposure due to putative distortion of the viral capsids bound to filters, the specificity of the antibody recognition was supported by immunogold labeling of virions bound to grids (Fig. 3C). When visualized at the EM level, the MVMp particles were profusely decorated with gold by the α-MVM and B7-MAb antibodies, while the latter antibody consistently failed to recognize chimeric virions. Importantly, MVM-P6L virions were again specifically recognized by the α-P6L antibody, although the ratio of gold particles per virion was low. In contrast, the α-A7R

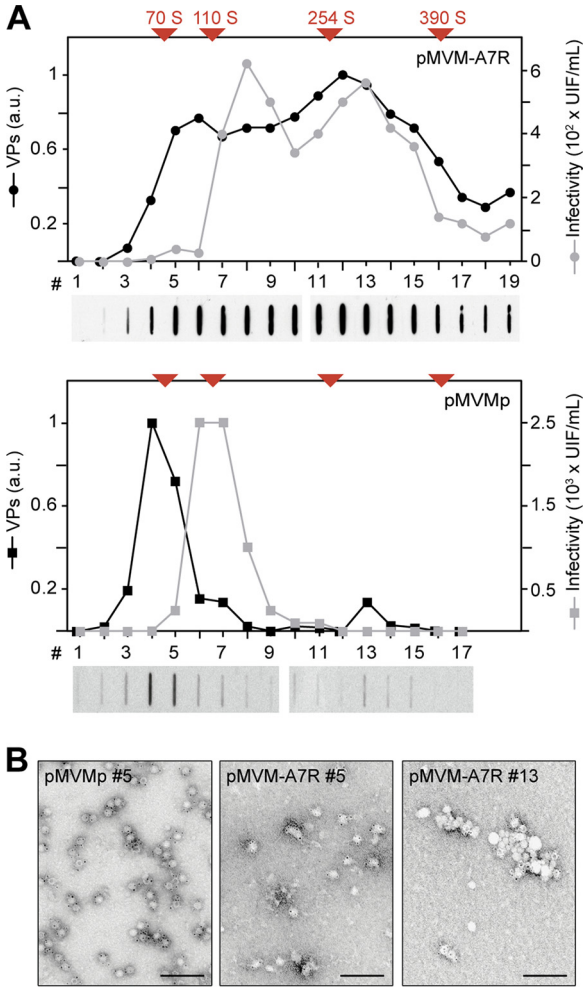

FIG 4 Assembly pattern of the chimeric virus MVM-A7R. Extracts from NB3245K cells transfected by the indicated genomic plasmids harvested at 48 hpt were sedimented for 1 h at 4°C through 5% to 30% sucrose gradients to resolve normal MVM particles and supraviral assemblies. (A) Slot-blot analysis of the distribution of the capsid proteins (VPs) in fractions loaded in PBS with 0.1% SDS and developed with the α-VP antibody. a.u., arbitrary units of densitometry. Samples were also studied for the distribution of infectivity (UIF). Shown are the average percentages of VP^+-expressing cells (α-VP antibody staining at 24 h postinoculation) scored under a microscope from two independent replicates. (B) EM analysis of the presence of viral particles and MVM assemblies in selected fractions from the sucrose gradients subjected to immunogold staining. The primary antibody was rabbit α-MVM capsid at 1:5 dilution. Scale bars, 100 nm.

antibody failed to decorate the MVM-A7R virions in multiple trials, even though the α-MVM antibody strongly decorated them (Fig. 3C, bottom). In summary, these analyses confirmed the efficient exposure and immune recognition of the P6L peptide displayed on the infectious MVM virion and also suggested that the subunits intertwining at the 3-fold axis of the capsid impose structural distortion(s) on the peptide A7R.

VEbp may impair MVM capsid assembly. We next investigated whether the restrictions imposed by the A7R peptide on virus genome packaging (Fig. 2B) and recovery of viral particles from transfections (Fig. 2C) could originate from a structural disturbance created in the MVM capsid. For this, the MVMp and MVM-A7R capsid assembly patterns were compared by sedimentation analysis through sucrose gradients of extracts from cells transfected by the respective genomic infectious plasmids (Fig. 4A) under conditions that resolved MVM particles and assembly intermediates. MVMp assembly showed a normal pattern of VP distribution in fractions corresponding to the sedimentation of empty capsids (70S), which accumulated at an S value slightly

lower than that of the bulk infectivity corresponding to the DNA-filled virus (110S) (Fig. 4A, bottom). In sharp contrast, the chimeric VP subunits and infectivity resulting from two independent pMVM-A7R transfections were consistently found distributed across a wide range of S values (Fig. 4A, top), with significant accumulation at fractions of normal viral size, but also at fractions of the 254S marker corresponding to molecular entities much larger than MVM particles. This unexpected pattern was carefully inspected for the presence of MVM-A7R large supraviral particles and assemblies by EM immunogold staining with an anti-MVM antibody. As illustrated in Fig. 4B, samples from distinct S values across the MVM-A7R gradients showed no evidence of large capsids or regular assemblies. Instead, the gold particles were confined in all samples to viral particles of normal size embedded within protein aggregates or misassembled VPs. This analysis demonstrated that A7R impairs the ordered MVM nuclear capsid assembly.

Antibody evasion and immunogenicity of MVM-VEbp chimeric viruses. We next analyzed whether the VEbp exposed on the capsid surface altered neutralization of the MVM chimeric viruses by specific antibodies (Fig. 5A). Infectious (UIF) MVMp and chimeric viruses were efficiently neutralized by the α-MVM polyclonal antiserum at high concentration, whereas the B7-MAb blocked only infection by the wt, as described previously (58, 59), failing to neutralize the chimeric viruses even at a high concentration. The capacity of MVM-P6L to absolutely evade B7-MAb neutralization was further confirmed by a PFU assay (Fig. 5B and C, left bars). Further PFU tests demonstrated that the MVM-P6L chimera indeed partially evaded neutralization by the α-MVM polyclonal antiserum when used at lower concentration (Fig. 5C, right bars). While the α-A7R antibody did not show neutralization capacity even against different stocks of MVM-A7R (Fig. 5A), the α-P6L polyclonal antibody at high concentration specifically decreased MVM-P6L infectivity. These results demonstrated the possibility of engineering an antibody footprint at the prominent 3-fold axis of the capsid with heterologous peptides that remain exposed on the surface and confer evasion of neutralization by α-MVM antibodies.

Another major aim of this research was the induction of α-VEGF antibodies using the MVM-VEbp as antigens. The α-P6L antibody weakly recognized native VEGF immobilized in filters (Fig. 3B, middle), consistent with the absence of immune interaction in the method originally used to select peptide P6L (15). We therefore addressed this issue with the MVM-A7R chimera, because peptide A7R was selected by the α-A7R MAb that efficiently binds (Fig. 3B, bottom) and neutralizes (13) native VEGF. To assay the immunogenicity of the VEbp presented in the context of the MVM capsid, we intraperitoneally (i.p.) injected mice with purified empty MVM-A7R capsids without adjuvant, and the specificity of the antisera was tested by dot blotting (Fig. 5D). Mice were sensitized to MVM capsid epitopes, as their sera efficiently recognized the wt and MVM-A7R capsids. Importantly, empty MVM-A7R capsids induced specific anti-VEGF antibodies, reacting with native VEGF immobilized on filters (Fig. 5D). This result supports replacement of 3-fold residues by VEbp as a successful strategy to mount an α-VEGF immune response with chimeric MVM capsids. Unexpectedly, repeated injections of equivalent amounts of infectious chimeric MVM-A7R virions did not induce significant levels of anti-VEGF antibodies (data not shown).

Genetic stability of chimeric MVM-VEbp. The capacity of MVM-A7R purified from passaged cultures to evade α-A7R antibody recognition (Fig. 3C and 5A), in spite of the specific α-A7R nuclear staining in pMVM-A7R-transfected cells (Fig. 3A) and the failure of MVM-A7R virions to induce α-VEGF antibodies in mice, prompted us to address the genetic stability of the chimeric capsids. The nucleotide sequences of loop 4, which harbors the residues replaced by the VEbp, and the other three loops (1 to 3) of the VPs forming the spike (Fig. 6A and B) were determined in populations of wt and chimeric viruses after 2 weeks of growth in culture, as well as in molecular and infectious biological clones. The sequences of loops 1 to 3 in populations harvested from transfection and isolated plaques showed no changes in respect to the reference sequence in any of the wt or chimeric viruses, indicating that manipulation of loop 4

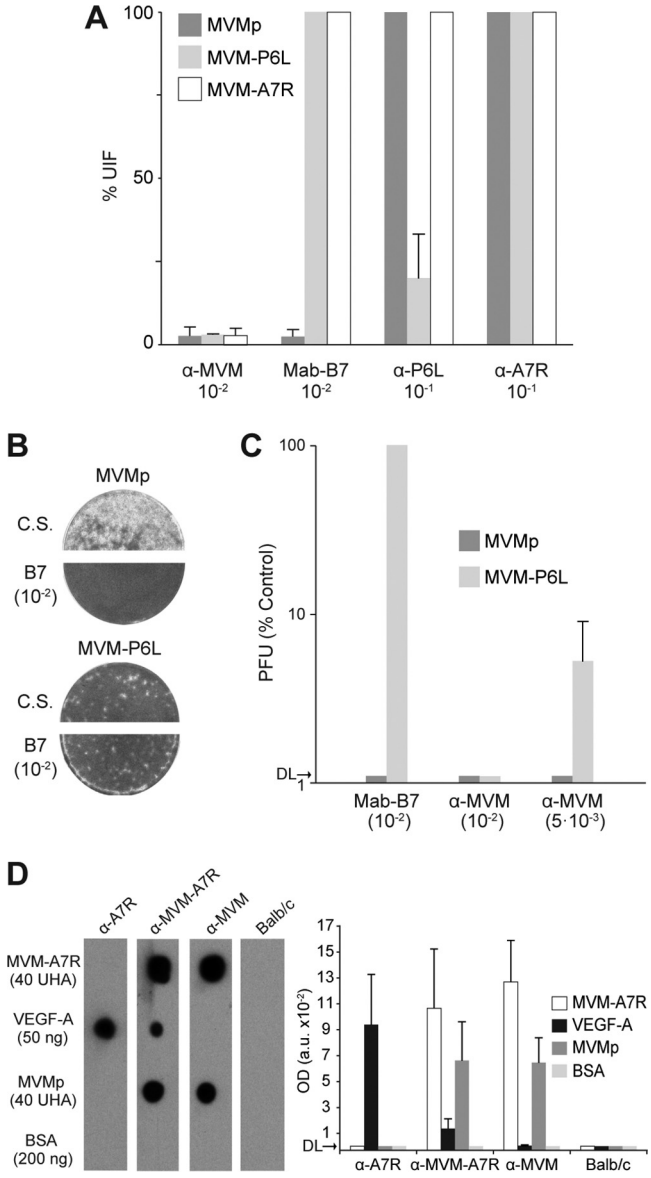

FIG 5 Evasion of antibody neutralization and immunogenicity of MVM-VEbp chimeras. (A) Neutralization assay of MVM-VEbp chimeras by specific antibodies. The viruses were incubated for 30 min in PBS with the indicated antibodies and inoculated onto NB342K cells, and their infectivity was determined by the number of VP-expressing cells (UIF) scored at 20 h postinoculation. The values are means and standard errors from five determinations. (B) MVM-P6L plaque-forming capacity evades B7-MAb neutralization. Shown are MVMp neutralization by B7-MAb in NB324K cells (top) and the lack of effect on chimeric MVM-P6L plaque-forming capacity at the same antibody dilution (bottom). C.S., control serum. (C) Comparison of neutralization of MVMp and MVM-P6L by the B7-MAb and α-MVM antibodies at the specified dilutions. Note the partial resistance of MVM-P6L to neutralization by the α-MVM antiserum. DL, detection limit of the assay. (D) Chimeric MVM-A7R capsids elicit anti-VEGF antibodies in BALB/c mice. (Left) Representative results of the antibody recognition (1:200 dilution) of the indicated amounts of each sample applied to nitrocellulose filters in PBS and developed by a chemiluminescence method. (Right) Antibody titers. Signals in the films were quantitated as for Fig. 4A. The values are means and standard errors from four independent immunizations ($n = 3$ mice per sample). OD, optical density; UHA, hemagglutination units.

by the VEbp did not select for any genetic modification in the rest of the loops forming the spike. The sequence of loop 4 in the MVM-P6L populations, and several biological clones (PFU), remained identical to that of the original genomic clone, with no evidence of heterogeneity (Fig. 6C). However, the sequences of loop 4 in samples from the MVM-A7R populations reflected genetic heterogeneity at nucleotide position 4016 in

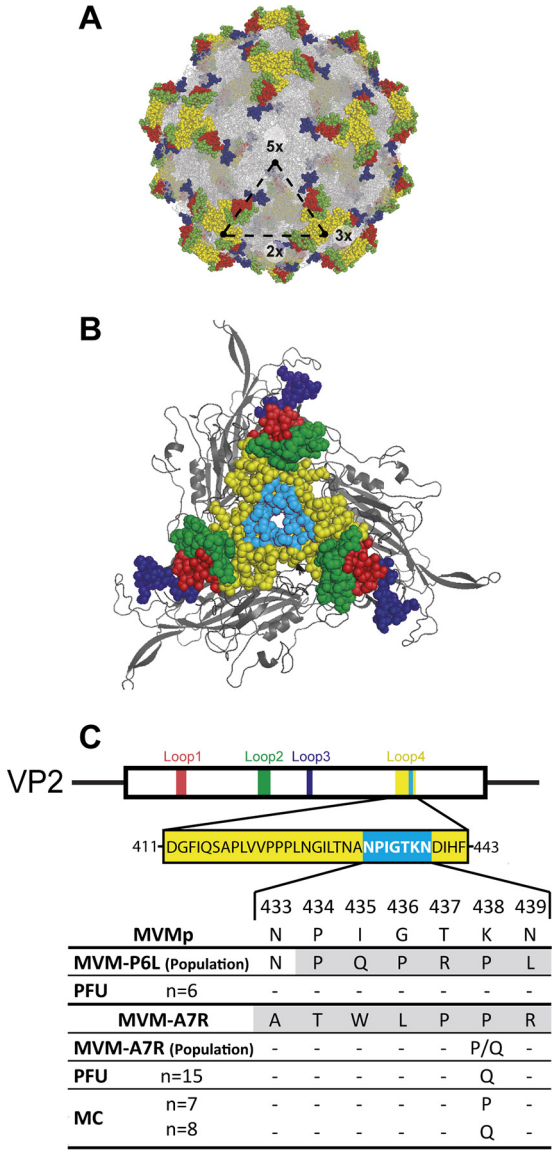

		433	434	435	436	437	438	439
MVMp		N	P	I	G	T	K	N
MVM-P6L (Population)		N	P	Q	P	R	P	L
PFU	n=6	-	-	-	-	-	-	-
MVM-A7R		A	T	W	L	P	P	R
MVM-A7R (Population)		-	-	-	-	-	P/Q	-
PFU	n=15	-	-	-	-	-	Q	-
MC	n=7	-	-	-	-	-	P	-
	n=8	-	-	-	-	-	Q	-

FIG 6 Genetic stability of the MVM-VEbp chimeras. (A) Icosahedral structure of the MVMp capsid (PyMol; PDB accession number 1z14) shown in stick representation (gray). The spike is shown as spheres colored at loop 1 (red), loop 2 (green), loop 3 (dark blue), and loop 4 (yellow). The locations of the 5-fold (5×), 3-fold (3×), and 2-fold (2×) symmetry axes are highlighted. (B) Enlarged top view of the topology of the loops forming the MVM spike. Substituted residues within loop 4 are shown in blue. (C) Genetic analysis of chimeric viruses grown in culture. The nucleotide sequences of the four loops were studied in the chimeric viruses grown in culture. The VP2 amino acid sequence forming loop 4 of the MVMp capsid is shown, and the residues replaced by the VEbp are highlighted. The average sequences of the MVM-P6L and MVM-A7R populations were obtained after 2 weeks in culture. The sequence of the initial MVM-A7R chimeric virus is outlined. PFU, virus biological clone; MC, molecular clone.

the chromatograms. A cytosine-to-adenosine mutation was observed (Fig. 6C), corresponding to a change of the second proline of the A7R peptide into glutamine (P6Q). This single mutation was apparent in several molecular clones constructed from the MVM-A7R population (see Materials and Methods): seven clones maintained adenosine, but eight showed cytosine at this position, supporting the heterogeneity observed in the population (Fig. 6C). Of note, the genetic analysis performed with biological clones (PFU) isolated from the MVM-A7R population consistently showed the P6Q change in all cases (Fig. 6C). Thus, peptide A7R in loop 4 of the spike impaired MVM plaque-forming capacity, but the single P6Q amino acid change selected in culture restored efficient plaque formation and fitness of the chimeric MVM-A7R-P6Q in culture.

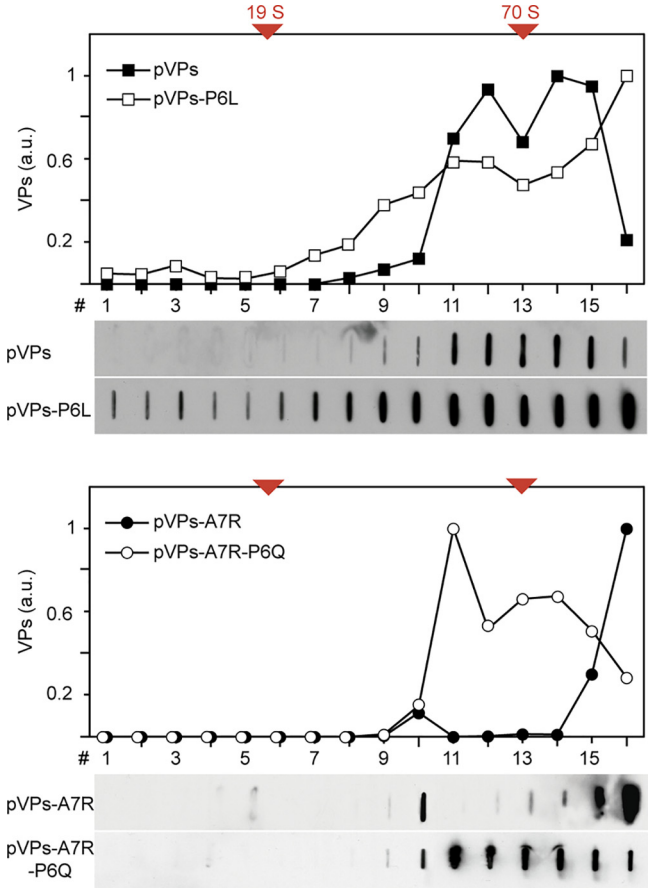

FIG 7 Pattern of chimeric empty-capsid assembly. Sedimentation analysis of VP assemblies expressed at 48 hpt in NB324K cells transfected by the specified plasmids. Samples were resolved by parallel centrifugation at 4°C through 5% to 30% sucrose gradients, and the amounts of VPs in the fractions were analyzed by slot-blot analysis as described in the legend to Fig. 4. (Top) Wt and chimeric P6L structural protein assemblies. (Bottom) Chimeric A7R and A7R-P6Q structural protein assemblies. The S values of the sedimentation markers (19S, thyroglobulin; 70S, empty MVM capsids) are indicated at the top. a.u., arbitrary units of densitometry.

Finally, we studied whether the restored plaque-forming capacity of the MVM-A7R-P6Q mutant was related to rescue of capsid assembly functions. For this, we compared the profiles of velocity sedimentation across sucrose gradients of the wt, chimeric, and A7R-P6Q capsid proteins in cells transfected by the respective VP-expressing plasmids (Fig. 7). The wt and chimeric VP-P6L proteins efficiently assembled in capsids with normal sedimentation values (Fig. 7, top). While chimeric VP-A7R proteins formed some capsids of normal size, they mostly were found in large assemblies or aggregates sedimenting at the bottom of the gradients (Fig. 7, bottom). This pattern was consistent with that observed after transfection of the genomic clones (Fig. 4), supporting the notion that the assembly defect of the MVM-A7R chimera is inherent to its VP subunits. Remarkably, the assembly pattern of the VP-A7R-P6Q subunits was similar to that of the wt, confirming P6Q as a compensatory mutation that provides a structural solution to the defective capsid assembly exhibited by MVM-A7R.

DISCUSSION

Two parallel areas of current clinical significance in cancer therapy, α-VEGF antibodies and oncolytic viruses, were combined in the present work aimed at endowing the infectious parvovirus MVM with potential antineovascularization properties. Infectious oncolytic parvoviruses displaying VEbp on the capsid surface could eventually be used as therapeutic vaccines to induce anti-VEGF neutralizing antibodies and thereby

inhibit neovascularization and tumor growth. The MVM capsid was engineered with two high-affinity VEbp within a major immunogenic epitope, and chimeric viruses were tested for infectivity, peptide exposure on assembled capsids, evasion of neutralization, induction of anti-VEGF antibodies, and genetic stability.

An infectious MVM-VEbp chimera. Replacement of viral sequences in loop 4 of the 3-fold axis capsid spike with the P6L peptide allowed propagation of the resulting chimeric virus in culture (Fig. 2A and C), consistent with its efficient genome replication and packaging (Fig. 2B), and a pattern of capsid assembly similar to that of wt MVM (Fig. 7, top). Preservation of major intracellular and extracellular capsid functions in the MVM-P6L life cycle was compatible with surface exposure of peptide P6L, allowing significant recognition (Fig. 3B and C) and neutralization (Fig. 5A) by the α-P6L polyclonal antibody. The configuration(s) of peptide P6L on the spike would favor novel contacts among the residues of the three VP subunits forming the spike in a structural solution that was genetically stable upon extensive viral passages in culture (Fig. 6). These data support loop 4 as a suitable site for the surface display of heterologous peptides on infectious MVM and structurally related parvoviruses.

VEbp may impair MVM nuclear capsid assembly. The infectivity of MVM-A7R, genome packaging, and capsid yield were severely hampered compared to wt MVM and MVM-P6L (Fig. 2). Genetic and biochemical analyses have shown that MVM assembly depends on translocation of trimeric intermediates across the nuclear envelope, driven by a structured nuclear localization motif (NLM) (28, 65–68). It was proposed that structured transport motifs may provide quality control for the capsid assembly pathway (67), which was also suggested for other parvoviruses (69, 70). The VP-A7R chimeric subunits accumulated in the nuclei of transfected cells (Fig. 3A), proving that the A7R peptide does not perturb NLM configuration and solvent exposure of the trimers. However, the VP-A7R subunits accumulated in the nucleus showed a patent assembly defect, composed of heterogeneous supraviral assemblies and/or aggregates with some viral particles embedded (Fig. 4). This pattern suggests that peptide A7R blocks the MVM assembly pathway at a structural switch that subunits must undergo to configure the 3-fold B7Mab binding epitope on the capsid surface (58), as this epitope is not formed by expressed (66) or isolated (28) trimers. Having two prolines in a row may impose high rigidity on peptide A7R, restricting the conformational flexibility required for subunits intertwining at the 3-fold axis (55, 56) to close the capsid shell. Aberrant contacts between the side chains of neighboring A7R residues on the 3-fold axis may lead to the misassembly and aggregation of subunits found in sedimentation analyses (Fig. 4 and 7). Previous evidence of peptide A7R structural rigidity was obtained when studying the VP2 and VP1 N termini running through the capsid channel that is required for MVM to initiate infection (52).

Immune interaction of MVM chimeras with the VEGF system. In our analysis of the constructed chimeras, VEbp-specific antibodies were used to demonstrate their exposure on the capsid and possible configuration restraints imposed by the folding and rearrangement of protein subunits accompanying capsid assembly. Peptide P6L was specifically recognized by the polyclonal anti-P6L antibody in chimeric VPs and purified viruses (Fig. 3 and 5A). P6L was selected as a VEGF mimic peptide binding neuropilin-1 and VEGF-R1 (15), but it has multiple interactive conformations and overlapping binding motifs (71). The recognition and partial neutralization of MVM-P6L by the polyclonal anti-P6L antibody indicates that capsid assembly does not mask all the P6L epitopes, although the precise configuration and immunogenicity of the remaining epitopes would require high-resolution structural analysis of the chimeric capsid.

The structure of peptide A7R in solution showed a significant secondary structure of the backbone that mimics the C-terminal domain of VEGF (72), and its native configuration could be traced with the α-A7R MAb (13) used in this study. A7R could be recognized weakly but specifically by this antibody in cells expressing chimeric VPs and filter-bound viral particles (Fig. 3A and B), but not in MVM-A7R virions bound to EM

grids (Fig. 3C). Furthermore, the α-A7R antibody failed to neutralize MVM-A7R grown in culture (Fig. 5A), as culturing resulted in a P6Q shift in the A7R sequence (Fig. 6) (see below). These data indicate that the native configuration of peptide A7R is severely constrained by a structural distortion imposed by MVM capsid at the 3-fold axis. However, MVM-A7R empty capsids induced anti-VEGF antibodies in mice (Fig. 5D), indicating that the inserted peptide A7R retains some native immunogenic epitopes. As the α-A7R MAb neutralized VEGF and showed antivascularization and tumor-inhibitory properties (14), it is expected that the anti-VEGF polyclonal antibodies induced in mice by the MVM-A7R chimeric capsid would harbor potent VEGF neutralization and tumor-inhibitory capacities, as well. The anticancer capacity of MVM-A7R-based vaccines, therefore, deserves further research.

A crucial issue for the therapeutic application of parvoviruses is preexisting immunity (73). Since the parvovirus capsid is highly immunogenic, neutralizing antibodies are prevalent in human and animal populations following natural exposures. For example, humoral immune response against MVM in tumor-bearing mice was shown to prevent viral transcription (74), and prospective patients seeking to enroll in gene therapy trials with AAV vectors must have low neutralizing anti-AAV antibody titers (e.g., ClinicalTrials.gov registration no. NCT01620801). Importantly, the prominent 3-fold axis of symmetry forms the major immunogenic domain of the antigenically better-studied parvoviral capsids (75–80), and thus, 3-fold chimeras should presumably harbor enhanced immune evasion capacity. Accordingly, in our study, the MVM-P6L and MVM-A7R chimeras were fully resistant to the B7-MAb that efficiently neutralized the wt (Fig. 5), and MVM-PL6 further partly evaded a powerful polyclonal neutralizing anti-MVM capsid antibody (Fig. 5C). Replacing the epitopes of neutralizing antibodies with heterologous peptides may delineate a fundamental approach toward the development of therapeutic parvoviruses with privileged immune evasion properties.

Parvovirus evolution can modify heterologous peptides. The genetic stability of chimeric capsids has received little attention during the extensive manipulation of parvovirus genomes and vectoring technology. We addressed the impact of evolution on the genetic stability of the MVM-VEbp chimeras, given the rapid MVM evolutionary response to other biological pressures exerted on the capsid, such as antibody neutralization (59, 81) and adaptive virulence (61, 62, 82). Replacement of wt residues within loop 4 by peptide A7R did not result in selection of compensatory mutations in the other loops forming the spike, which may reflect their lack of contact with the engineered region (Fig. 6B). However, extensive passaging of MVM-A7R in culture did select for the P6Q single-amino-acid change within the engineered peptide, which restored capsid assembly efficiency (Fig. 7) and plaque-forming capacity (Fig. 6). This evolutionary change explains the slow progression of MVM-A7R in culture compared to the wt and MVM-P6L (Fig. 2A), as it needs to undergo the P6Q selection process, and also may explain the poor recognition (Fig. 3C) and neutralization (Fig. 5A) by the anti-A7R antibody. The P6Q change was consistently found in two independent cultures of MVM-A7R, suggesting that it is a highly preferred structural solution to overcome its assembly defect. An MVM-A7R-P6Q capsid structure resolved at high resolution may explain how contacts driven by the disposition of the glutamine side chain stabilize the VP subunit interactions at the 3-fold axis of the chimeric spike. Further, the assembly-escape P6Q mutant may inspire minimal genetic interventions to successfully overcome structural restrictions imposed by manipulations of the 3-fold axis. These observations also raise biosafety concerns for the large-scale therapeutic delivery of infectious parvovirus chimeras and replicative vectors.

Concluding remarks. This study shows that replacement of wt short amino acid sequences by heterologous peptides, and not merely insertions, is an optimal strategy to engineer the capsid of parvoviruses. The approach was illustrated in the engineering of oncolytic MVM with antiangiogenic VEbp, which endowed infectious chimeric viruses with the capacity to induce α-VEGF antibodies and to evade neutralization by α-MVM antibodies. Current efforts are focused on testing MVM-VEbp antineovascular-

ization and antitumor properties. These chimeric oncolytic viruses may bring important therapeutic benefits over passive α-VEGF antibody regimes for immunocompetent cancer patients. We also demonstrated that the flexibility of introduced peptide sequences may impose severe structural restrictions on capsid assembly, which may lead to spontaneous selection of variants with enhanced viability. Conversely, subunit contact and intertwining at the 3-fold axis of the capsid may alter peptide configurations, partly disabling their immunogenic functions. These findings may be of paramount relevance to ongoing development of parvoviral cancer and gene therapy applications. We speculate that peptides with fewer structural requirements, or insertions in other capsid domains with different surface topologies, might overcome these restrictions. However, on the basis of this study and the dynamic evolution of these ssDNA viruses, we anticipate that isolation of genetically stable replicative parvoviruses exposing heterologous peptides in immunodominant capsid domains will remain a challenging task.

MATERIALS AND METHODS

Cells and viruses. The NB324K simian virus 40 (SV40)-transformed human newborn kidney cell line (83) was maintained in Dulbecco's modified Eagle medium (DMEM) supplemented with 5% fetal calf serum (Gibco BRL). For routine transfections 3×10^6 cells were electroporated with 10 μg of plasmid following a previously described method (84), but the growth of chimeric viruses usually required transfection at a large scale (52).

The prototype (p) strain of the *Protoparvovirus* MVM (19, 24) was used in this study. Viral stocks of MVMp and chimeric viruses were harvested 48 hpt and purified from cellular pellets by sucrose cushions and cesium chloride equilibrium centrifugation, as previously described (50, 52, 85). Viral particles in fractions corresponding to the density of DNA-filled virus were pooled, dialyzed against phosphate-buffered saline (PBS), and kept at −70°C in aliquots. The MVM-A7R chimeric DNA-filled virus preparations were concentrated by centrifugation at 4°C in Amicon Ultra-15 filters (Millipore) as recommended by the manufacturer. The titers of infectious viruses were determined by a standard PFU assay (50) or by determining the number of VP-expressing cells (units of immunofluorescence; UIF) by inoculating NB324K cell monolayers grown on coverslips with duplicate serial dilutions, as previously described (52, 84). The amounts of structural proteins in purified virus preparations (Fig. 3B) were determined by SDS-PAGE using bovine serum albumin (BSA) as a standard (52). The limiting amounts of MVM-A7R virions were determined by hemagglutination to mouse erythrocytes (86) using the homologous empty capsid as a reference. Virus genome replication was monitored by Southern blotting using 1% agarose gels loaded with low-molecular-weight DNA (84) obtained from electroporated NB324K cells. Samples were alkali blotted to filters and hybridized with an MVM full-length probe labeled by random priming using a DIG High Prime DNA-labeling and detection starter kit II (Roche Applied Science) according to the manufacturer's protocol.

Construction of MVM-VEbp chimeras. Spike virus chimeras were constructed by mutagenesis. The MVM-P6L chimera has the P434-N439 VP2 residues deleted and replaced by the peptide P6L residues PQPRPL (nucleotides 4093 to 4111 were replaced by 5′-CAGCCACGCCCACTG-3′). The MVM-A7R chimera has the VP2 residues N433 to N439 deleted and replaced by the peptide A7R residues ATWLPPR (nucleotides 4090 to 4111, 5′-AACCCTATTGGGACTAAAAAT-3′, were substituted by directed mutagenesis for 5′- GCCACGTGGCTGCCGCCGAGG-3′). The DNA template used in all the mutants was the pSVtk-VPs (87), which expresses the VP1 and VP2 proteins of MVMp under the control of the SV40-thymidine kinase enhancer-promoter. Flanking oligonucleotides used at the 5′ and 3′ extremes were S1 (5′-GGGGAATT CGCTCAAGGGAGCAGACATGG-3′) and S2 (5′-GTAACAATTCTAGAAAGTGTGGCTCCG-3′), corresponding to nucleotides 3721 to 3740 with an EcoRI site inserted upstream of nucleotide 3721, in the S1 primer, and nucleotides 4329 to 4355 of the MVM genome sequence in the S2 primer. To insert the different peptides, we used V3A (5′-CAGTGGGCGTGGCTGAGGGTTTGCATTTGTAAGAATG-3′) and V4A (5′-CCTCAG CCACGCCCACTGGACATTCATTTTTCAAATG-3′) for peptide P6L and V3C (5′-CCTCGGCGGCAGCCACGTGG CTGCATTTGTAAGAATGCC-3′) and V4C (5′-GCCACGTGGCTGCCGCCGAGGGACATTCATTTTTCAAATG-3′) to insert peptide A7R. High-fidelity Platinum *Pfx* (Invitrogen) and *Pwo* (Roche) polymerases were used with the PCR programs of the manufacturer. The amplified fragments were cloned into pUC19 by digestion with the EcoRI and XbaI restriction enzymes and then cloned into the pMM984 infectious plasmid (63) between the HpaI and XbaI restriction sites (nucleotides 3759 to 4342). Genomic plasmids were always grown from a single transformed colony of *Escherichia coli* JC8111, a bacterial strain that permits deletion-resistant propagation of MVM plasmid clones bearing terminal palindromes (88), and sequenced to verify the absence of additional mutations. Plasmids were purified on a large scale with Plasmid Maxi kits (Qiagen) using the manufacturer's protocol.

The pSV-VP-P6L, pSV-VP-A7R, and pSV-VP-A7R-P6Q plasmid clones were constructed by replacing the respective amplified EcoRI-XbaI fragments mentioned above with the HpaI-XbaI fragment (nucleotides 3759 to 4342) of the pSVtk-VPs plasmid (87). These plasmids were transformed into and purified from the *E. coli* DH5α bacteria.

Antibodies. The MVM antibodies used in this work have been previously described: the α-VP rabbit polyclonal antiserum was raised in rabbit against denatured VP2 and used for the general localization of

the VP1 and VP2 proteins independently of the configuration (65); the B7 mouse monoclonal antibody (B7-MAb), which recognizes an epitope configured by an intact empty capsid and DNA-filled virus localized at the 3-fold axes (58, 59) but fails to react with isolated VP subunits or trimers (28, 66); and the α-MVM antibody raised in rabbit against the native capsid and used to recognize mainly conformational epitopes (67, 89).

Specific antibodies of the VEGF system were as follows: the α-P6L rabbit polyclonal antibody was raised against the 12-mer PQPRPLPQPRPL peptide sequence (a dimer of the P6L peptide) coupled to keyhole limpet hemocyanin (KLH) and administered by injection (100 μg per dose) in a first dose emulsified in Freund´s complete adjuvant followed by two boost injections in incomplete adjuvant. Bleeding was done 10 days after the last injection, and the serum was affinity purified (NAb protein G; Thermo); the α-A7R antibody corresponds to a commercial α-VEGF mouse monoclonal antibody (Sigma; V4758) that binds human native VEGF and neutralizes its biological activity. This antibody was used to identify by phage display the 7-mer ATWLPPR anti-angiogenic A7R peptide binding neuropilin-1 (13). Recombinant biologically active human VEGF-A (Peprotech 100-20) was used to control the α-A7R antibody activity.

Immunological methods. Double-label indirect IF was performed with cells seeded onto glass coverslips following previously described protocols (65). Secondary antibodies (Jackson Immunoresearch; used at 1/1,000 dilution) were an α-rabbit IgG conjugated to Texas Red (TXRD) and an α-mouse IgG conjugated to fluorescein isothiocyanate (FITC). Slot-dot analysis under vacuum was performed as recommended by the manufacturer (Hoeffer) with nitrocellulose membranes (Scheider and Schull) and applying samples under native conditions diluted in PBS (Fig. 3B and 5D) or in denatured configuration diluted in PBS with 0.1% SDS for best VP quantitation (Fig. 4A and 7). Filters were developed as described above with the primary antibodies indicated in the figures and secondary anti-rabbit or anti-mouse antibodies, IgGs conjugated with peroxidase.

For mouse immunization, 8-week-old BALB/c mice were injected in the tail vein with wt MVMp and chimeric (MVM-P6L or MVM-A7R) purified capsids and DNA-filled virions. A single injection of 1 μg of viral particles in 100 μl of PBS without adjuvant was administered per mouse, and whole blood was collected 1 month postinjection. The blood was coagulated at 37°C for 20 min and centrifuged at 2,000 $\times$ *g* for 10 min at 4°C, and the serum was heat inactivated at 55°C for 15 min and stored in aliquots at −70°C.

Electron microscopy. Virus particles were adsorbed for 15 min to glow-discharged collodion/carbon-coated copper grids, washed with water, and negatively stained for 50 s with 2% uranyl acetate before visualization. For immunogold labeling, the grid-adsorbed particles were incubated for 30 min with the primary antibodies at dilutions indicated in the figure legends. Bound antibodies were labeled for 30 min with protein A conjugated to 5-nm gold particles (EM Laboratory, Utrecht University, Utrecht, The Netherlands) or a goat anti-mouse IgG conjugated to 5-nm gold particles (British Biocell International). Finally, specimens were negatively stained with 2% uranyl acetate and visualized under a JEOL (Tokyo, Japan) JEM-1010 electron microscope equipped with a TVIPS F416 camera (Gauting, Germany).

Genetic analyses. To study chimeric-virus evolution, low-molecular-weight DNA was prepared as described previously (87) from MVM-A7R stocks and infected cell cultures and used as a template to obtain molecular clones by PCR amplification with the primers vVP-3 (5′-CGCACTAGACCACCTGC-3′) and VPSeq-1 (5′-GTTTCCAGTAGCAGTTGG-3′). The product was digested with NspI restriction enzyme, the VP2 fragment encompassing the four loops of the spike was cloned into pUC19 at the SphI site and transformed into the DH5α strain of *E. coli*, and plasmids were purified from the bacterial clones (Wizard Plus SV minipreps; Promega). Infectious MVM, MVM-P6L, and MVM-A7R clones were isolated from plaques (PFU) formed in NB324K cell monolayers stained with phenyl red in low gelling point (LM-GCT) agarose. Each viral clone was incubated in 100 μl of Tris (50 mM, pH 7.5) at 4°C overnight, clarified by centrifugation, and stored at −20°C. Samples were amplified using GoTaq Green Master Mix (Promega) and the vVP4 (2945 to 2961; 5′-CGCATTATAGATTCTTG-3′), vVP-3 (2704 to 2720; 5′-CGCACTAGACCACC TGC-3′), and VPSeq-2 (5′-CCATTTAGTGGTGGTGG-3′) primers to amplify the regions containing loops 1, 2, and 3 and the vVP-8 (5′-GCCAATGGCAGTGTTAG-3′) and VPSeq-1 (4489 to 4506; 5′-GTTTCCAGTAGC AGTTGG-3′) primers for the region of loop 4. The amplified DNA fragments were cut off and purified (Wizard SV Gel and PCR Clean-Up System; Promega) from the agarose gels and sequenced by automated sequencing. Mutations were confirmed by two rounds of sequence analysis with DNAStar Lasergene v7.1.0 and BioEdit sequence alignment editor v7.0.9.0 software.

Capsid assembly. To characterize capsid assembly patterns, genomic (wt or chimeric) plasmids, as well as plasmids expressing VPs only (pSVtk-VP derivatives), were transfected into NB324K cells, and protein extracts were subjected to sedimentation analysis performed as described previously (66). In brief, transfected cells washed with PBS were scraped in 50 mM HEPES, pH 8.0, 150 mM NaCl, 2 mM $MgCl_2$, 1 mM EDTA (HNEM buffer) supplemented with protease (0.1 mM phenylmethylsulfonyl fluoride [PMSF], 10 μg/ml leupeptin, 10 μg/ml pepstatin, 10 μg/ml aprotinin, 100 μg/ml TPCK [tosylsulfonyl phenylalanyl chloromethyl ketone]) and phosphatase (20 mM glycerol phosphate, 5 mM NaF) inhibitors and disrupted in a cooled water bath sonicator. The cellular lysates were clarified by centrifugation at 15,000 $\times$ *g* and 4°C for 30 min in a benchtop centrifuge, layered onto 14 ml of 5% to 30% sucrose gradients prepared in HNEM, and ultracentrifuged at 160,000 $\times$ *g* in a SW40 rotor (Beckman) at 5°C for 6 h for the analysis of capsid formation or 1 h for supraviral assemblies and aggregates. The molecular size markers were thyroglobulin (669 kDa; 19S; Sigma) and the following gradient-purified viral particles: MVMp empty capsid (70S), MVMp DNA-filled virion (110S), and ϕ29 (254S) and λ (390S) bacteriophages. Fractions were tested for infectivity (UIF), and VP amounts by slot-blotting (Hoefer) applying the samples under vacuum onto nitrocellulose membranes and developed with the α-VP polyclonal antibody. For quantitation of VP signals, films were scanned with a densitometer (Bio-Rad GS-900), and the relative

band intensities were determined with Image Lab v.5.2 (Bio-Rad). For EM inspection, fractions were dialyzed against PBS and concentrated by centrifugation in Centricon Ultracel YM-30 filters (Millipore) at 4°C, as recommended by the manufacturer, prior to immunogold labeling.

SUPPLEMENTAL MATERIAL

Supplemental material for this article may be found at https://doi.org/10.1128/JVI.00798-19.

SUPPLEMENTAL FILE 1, MOV file, 12 MB.

SUPPLEMENTAL FILE 2, PDF file, 0.04 MB.

ACKNOWLEDGMENTS

E.G., C.S.-M., and T.C.-L. contributed equally to this work.

We are indebted to P. Tattersall (Yale University, New Haven, CT) for generously providing the original pMM984 molecular clone of MVMp. Technical support by J. González-Nicolás is also acknowledged.

T.C.-L. is the recipient of a contract from Comunidad de Madrid (PEJ16/MED/AI-0818), and G.A. is supported by the Amarouto Program (Comunidad de Madrid). This work was supported by the following grants: contract QLK3-CT-2001-01010 (European Commission), SAF2011-29403 (Spanish Ministerio de Ciencia e Innovación), SAF2015-68522-P-MINECO/FEDER, UE (Spanish Ministerio de Economía y Competitividad and Ministerio de Ciencia, Investigación y Universidades), and S2013/ABI-2906-FEDER (Comunidad de Madrid) to J.M.A. and institutional grants from the Fundación Ramón Areces and Banco Santander to the Centro de Biología Molecular Severo Ochoa (CSIC-UAM).

REFERENCES

1. Plate KH, Breier G, Weich HA, Risau W. 1992. Vascular endothelial growth factor is a potential tumour angiogenesis factor in human gliomas *in vivo*. Nature 359:845–848. https://doi.org/10.1038/359845a0.
2. Carmeliet P, Jain RK. 2011. Molecular mechanisms and clinical applications of angiogenesis. Nature 473:298–307. https://doi.org/10.1038/nature10144.
3. Robinson CJ, Stringer SE. 2001. The splice variants of vascular endothelial growth factor (VEGF) and their receptors. J Cell Sci 114:853–865.
4. Dings RP, Vang KB, Castermans K, Popescu F, Zhang Y, Oude Egbrink MG, Mescher MF, Farrar MA, Griffioen AW, Mayo KH. 2011. Enhancement of T-cell mediated antitumor response: angiostatic adjuvant to immunotherapy against cancer. Clin Cancer Res 17:3134–3145. https://doi.org/10.1158/1078-0432.CCR-10-2443.
5. Schoenfeld JD, Dranoff G. 2011. Anti-angiogenesis immunotherapy. Hum Vaccin 7:976–981. https://doi.org/10.4161/hv.7.9.16407.
6. Shih T, Lindley C. 2006. Bevacizumab: an angiogenesis inhibitor for the treatment of solid malignancies. Clin Ther 28:1779–1802. https://doi.org/10.1016/j.clinthera.2006.11.015.
7. Sandler A, Gray R, Perry MC, Brahmer J, Schiller JH, Dowlati A, Lilenbaum R, Johnson DH. 2006. Paclitaxel-carboplatin alone or with bevacizumab for non-small-cell lung cancer. N Engl J Med 355:2542–2550. https://doi.org/10.1056/NEJMoa061884.
8. Ferrara N, Adamis AP. 2016. Ten years of anti-vascular endothelial growth factor therapy. Nat Rev Drug Discov 15:385–403. https://doi.org/10.1038/nrd.2015.17.
9. Wentink MQ, Hackeng TM, Tabruyn SP, Puijk WC, Schwamborn K, Altschuh D, Meloen RH, Schuurman T, Griffioen AW, Timmerman P. 2016. Targeted vaccination against the bevacizumab binding site on VEGF using 3D-structured peptides elicits efficient antitumor activity. Proc Natl Acad Sci U S A 113:12532–12537. https://doi.org/10.1073/pnas.1610258113.
10. Yang Y, Zhang Y, Cao Z, Ji H, Yang X, Iwamoto H, Wahlberg E, Länne T, Sun B, Cao Y. 2013. Anti-VEGF- and anti-VEGF receptor-induced vascular alteration in mouse healthy tissues. Proc Natl Acad Sci U S A 110:12018–12023. https://doi.org/10.1073/pnas.1301331110.
11. Gavilondo JV, Hernández-Bernal F, Ayala-Ávila M, de la Torre AV, de la Torre J, Morera-Díaz Y, Bequet-Romero M, Sánchez J, Valenzuela CM, Martín Y, Selman-Housein KH, Garabito A, Lazo OC, CENTAURO Group of Investigators. 2014. Specific active immunotherapy with a VEGF vaccine in patients with advanced solid tumors. Results of the CENTAURO antigen dose escalation phase I clinical trial. Vaccine 32:2241–2250. https://doi.org/10.1016/j.vaccine.2013.11.102.
12. Vicari D, Foy KC, Liotta EM, Kaumaya PT. 2011. Engineered conformation-dependent VEGF peptide mimics are effective in inhibiting VEGF signaling pathways. J Biol Chem 286:13612–13625. https://doi.org/10.1074/jbc.M110.216812.
13. Binétruy-Tournaire R, Demangel C, Malavaud B, Vassy R, Rouyre S, Kraemer M, Plouët J, Derbin C, Perret G, Mazié JC. 2000. Identification of a peptide blocking vascular endothelial growth factor (VEGF)-mediated angiogenesis. EMBO J 19:1525–1533. https://doi.org/10.1093/emboj/19.7.1525.
14. Starzec A, Vassy R, Martin A, Lecouvey M, Di Benedetto M, Crépin M, Perret GY. 2006. Antiangiogenic and antitumor activities of peptide inhibiting the vascular endothelial growth factor binding to neuropilin-1. Life Sci 79:2370–2381. https://doi.org/10.1016/j.lfs.2006.08.005.
15. Giordano RJ, Cardó-Vila M, Lahdenranta J, Pasqualini R, Arap W. 2001. Biopanning and rapid analysis of selective interactive ligands. Nat Med 7:1249–1253. https://doi.org/10.1038/nm1101-1249.
16. Pan Q, Chanthery Y, Liang WC, Stawicki S, Mak J, Rathore N, Tong RK, Kowalski J, Yee SF, Pacheco G, Ross S, Cheng Z, Le Couter J, Plowman G, Peale F, Koch AW, Wu Y, Bagri A, Tessier-Lavigne M, Watts RJ. 2007. Blocking neuropilin-1 function has an additive effect with anti-VEGF to inhibit tumor growth. Cancer Cell 11:53–67. https://doi.org/10.1016/j.ccr.2006.10.018.
17. Miest TS, Cattaneo R. 2014. New viruses for cancer therapy: meeting clinical needs. Nat Rev Microbiol 12:23–34. https://doi.org/10.1038/nrmicro3140.
18. Bell J, McFadden G. 2014. Viruses for tumor therapy. Cell Host Microbe 15:260–265. https://doi.org/10.1016/j.chom.2014.01.002.
19. Cotmore SF, Agbandje-McKenna M, Chiorini JA, Mukha DV, Pintel DJ, Qiu J, Soderlund-Venermo M, Tattersall P, Tijssen P, Gatherer D, Davison AJ. 2014. The family *Parvoviridae*. Arch Virol 159:1239–1247. https://doi.org/10.1007/s00705-013-1914-1.
20. Toolan HW, Rhode SL, III, Gierthy JF. 1982. Inhibition of 7, 12-dimethylbenz(a)anthrocene-induced tumors in Syrian hamster by prior infection with H-1 parvovirus. Cancer Res 42:2552–2555.
21. Rommelaere J, Geletneky K, Angelova AL, Daeffler L, Dinsart C, Kiprianova I, Schlehofer JR, Raykov Z. 2010. Oncolytic parvoviruses as cancer

therapeutics. Cytokine Growth Factor Rev 21:185–195. https://doi.org/10.1016/j.cytogfr.2010.02.011.
22. Santiago-Ortiz JL, Schaffer DV. 2016. Adeno-associated virus (AAV) vectors in cancer gene therapy. J Control Release 240:287–301. https://doi.org/10.1016/j.jconrel.2016.01.001.
23. Geletneky K, Hajda J, Angelova AL, Leuchs B, Capper D, Bartsch AJ, Neumann JO, Schöning T, Hüsing J, Beelte B, Kiprianova I, Roscher M, Bhat R, von Deimling A, Brück W, Just A, Frehtman V, Löbhard S, Terletskaia-Ladwig E, Fry J, Jochims K, Daniel V, Krebs O, Dahm M, Huber B, Unterberg A, Rommelaere J. 2017. Oncolytic H-1 parvovirus shows safety and signs of immunogenic activity in a first phase I/IIa glioblastoma trial. Mol Ther 25:2620–2634. https://doi.org/10.1016/j.ymthe.2017.08.016.
24. Crawford LV. 1966. A minute virus of mice. Virology 29:605–612. https://doi.org/10.1016/0042-6822(66)90284-4.
25. Segovia JC, Real A, Bueren J, Almendral JM. 1991. *In vitro* myelosuppressive effects of the parvovirus minute virus of mice (MVMi) on hematopoietic stem and committed progenitor cells. Blood 77:980–988.
26. Mousset S, Rommelaere J. 1982. Minute virus of mice inhibits cell transformation by simian virus 40. Nature 300:537–539. https://doi.org/10.1038/300537a0.
27. Rubio MP, Guerra S, Almendral JM. 2001. Genome replication and postencapsidation functions mapping to the non-structural gene restrict the host range of a murine parvovirus in human cells. J Virol 75:11573–11582. https://doi.org/10.1128/JVI.75.23.11573-11582.2001.
28. Riolobos L, Valle N, Hernando E, Maroto B, Kann M, Almendral JM. 2010. Viral oncolysis that targets Raf-1 signaling control of nuclear transport. J Virol 84:2090–2099. https://doi.org/10.1128/JVI.01550-09.
29. Ventoso I, Berlanga JJ, Almendral JM. 2010. Translation control by protein kinase R restricts minute virus of mice infection: role in parvovirus oncolysis. J Virol 84:5043–5051. https://doi.org/10.1128/JVI.02188-09.
30. Paglino JC, Ozduman K, van den Pol AN. 2012. LuIII parvovirus selectively and efficiently targets replicates in, and kills human glioma cells. J Virol 86:7280–7291. https://doi.org/10.1128/JVI.00227-12.
31. Guetta E, Graziani Y, Tal J. 1986. Suppression of Ehrlich ascites tumors in mice by minute virus of mice. J Natl Cancer Inst 76:1177–1180.
32. Arulanandam R, Batenchuk C, Angarita FA, Ottolino-Perry K, Cousineau S, Mottashed A, Burgess E, Falls TJ, De Silva N, Tsang J, Howe GA, Bourgeois-Daigneault M-C, Conrad DP, Daneshmand M, Breitbach CJ, Kirn DH, Raptis L, Sad S, Atkins H, Huh MS, Diallo J-S, Lichty BD, Ilkow CS, Le Boeuf F, Addison CL, McCart JA, Bell JC. 2015. VEGF-mediated induction of PRD1-BF1/Blimp1expression sensitizes tumor vasculature to oncolytic virus infection. Cancer Cell 28:210–224. https://doi.org/10.1016/j.ccell.2015.06.009.
33. Thorne SH, Tam BYY, Kirn DH, Contag CH, Kuo CJ. 2006. Selective intratumoral amplification of an antiangiogenic vector by an oncolytic virus produces enhanced antivascular and anti-tumor efficacy. Mol Ther 13:938–946. https://doi.org/10.1016/j.ymthe.2005.12.010.
34. Yu DC, Lee JS, Yoo JY, Shin H, Deng H, Wei Y, Yun CO. 2012. Soluble vascular endothelial growth factor decoy receptor FP3 exerts potent antiangiogenic effects. Mol Ther 20:938–947. https://doi.org/10.1038/mt.2011.285.
35. Watanabe M, Boyer JL, Crystal RG. 2010. AAVrh.10-mediated genetic delivery of bevacizumab to the pleura to provide local anti-VEGF to suppress growth of metastatic lung tumors. Gene Ther 17:1042–1051. https://doi.org/10.1038/gt.2010.87.
36. Xie Y, Hicks MJ, Kaminsky SM, Moore MA, Crystal RG, Rafii A. 2014. AAV-mediated persistent bevacizumab therapy suppresses tumor growth of ovarian cancer. Gynecol Oncol 135:325–332. https://doi.org/10.1016/j.ygyno.2014.07.105.
37. Sedlik C, Saron M, Sarraseca J, Casal I, Leclerc C. 1997. Recombinant parvovirus-like particles as an antigen carrier: a novel nonreplicative exogenous antigen to elicit protective antiviral cytotoxic T cells. Proc Natl Acad Sci U S A 94:7503–7508. https://doi.org/10.1073/pnas.94.14.7503.
38. Rueda P, Hurtado A, del Barrio M, Martinez-Torrecuadrada JL, Kamstrup S, Leclerc C, Casal JI. 1999. Minor displacements in the insertion site provoke major differences in the induction of antibody responses by chimeric parvovirus-like particles. Virology 263:89–99. https://doi.org/10.1006/viro.1999.9911.
39. Rodríguez D, González-Aseguinolaza G, Rodríguez JR, Vijayan A, Gherardi M, Rueda P, Casal JI, Esteban M. 2012. Vaccine efficacy against malaria by the combination of porcine parvovirus-like particles and vaccinia virus vectors expressing CS of Plasmodium. PLoS One 7:e34445. https://doi.org/10.1371/journal.pone.0034445.
40. Rybniker J, Nowag A, Janicki H, Demant K, Hartmann P, Büning H. 2012. Incorporation of antigens into viral capsids augments immunogenicity of adeno-associated virus vector-based vaccines. J Virol 86:13800–13804. https://doi.org/10.1128/JVI.01708-12.
41. Girod A, Ried M, Wobus C, Lahm H, Leike K, Kleinschmidt J, Deleage G, Hallek M. 1999. Genetic capsid modifications allow efficient re-targeting of adeno-associated virus type 2. Nat Med 5:1438. https://doi.org/10.1038/71021.
42. Shi W, Arnold GS, Bartlett JS. 2001. Insertional mutagenesis of the adeno-associated virus type 2 (AAV2) capsid gene and generation of AAV2 vectors targeted to alternative cell-surface receptors. Hum Gene Ther 12:1697–1711. https://doi.org/10.1089/104303401750476212.
43. Muller OJ, Kaul F, Weitzman MD, Pasqualini R, Arap W, Kleinschmidt JA, Trepel M. 2003. Random peptide libraries displayed on adeno-associated virus to select for targeted gene therapy vectors. Nat Biotechnol 21:1040–1046. https://doi.org/10.1038/nbt856.
44. Warrington KH, Jr, Gorbatyuk OS, Harrison JK, Opie SR, Zolotukhin S, Muzyczka N. 2004. Adeno-associated virus type 2 VP2 capsid protein is nonessential and can tolerate large peptide insertions at its N terminus. J Virol 78:6595–6609. https://doi.org/10.1128/JVI.78.12.6595-6609.2004.
45. Asokan A, Conway JC, Phillips JL, Li C, Hegge J, Sinnott R, Yadav S, DiPrimio N, Nam HJ, Agbandje-McKenna M, McPhee S, Wolff J, Samulski RJ. 2010. Reengineering a receptor footprint of adeno-associated virus enables selective and systemic gene transfer to muscle. Nat Biotechnol 28:79–82. https://doi.org/10.1038/nbt.1599.
46. Lisowski L, Dane AP, Chu K, Zhang Y, Cunningham SC, Wilson EM, Nygaard S, Grompe M, Alexander IE, Kay MA. 2014. Selection and evaluation of clinically relevant AAV variants in a xenograft liver model. Nature 506:382–386. https://doi.org/10.1038/nature12875.
47. Paulk NK, Pekrun K, Zhu E, Nygaard S, Li B, Xu J, Chu K, Leborgne C, Dane AP, Haft A, Zhang Y, Zhang F, Morton C, Valentine MB, Davidoff AM, Nathwani AC, Mingozzi F, Grompe M, Alexander IE, Lisowski L, Kay MA. 2018. Bioengineered AAV capsids with combined high human liver transduction *in vivo* and unique humoral seroreactivity. Mol Ther 26:289–303. https://doi.org/10.1016/j.ymthe.2017.09.021.
48. Carreira A, Menendez M, Reguera J, Almendral JM, Mateu MG. 2004. *In vitro* disassembly of a parvovirus capsid and effect on capsid stability of heterologous peptide insertions in surface loops. J Biol Chem 279:6517–6525. https://doi.org/10.1074/jbc.M307662200.
49. Hurtado A, Rueda P, Nowicky J, Sarraseca J, Casal JI. 1996. Identification of domains in canine parvovirus VP2 essential for the assembly of virus-like particles. J Virol 70:5422–5429.
50. Gil-Ranedo J, Hernando E, Valle N, Riolobos L, Maroto B, Almendral JM. 2018. Differential phosphorylation and N-terminal configuration of capsid subunits in parvovirus assembly and viral trafficking. Virology 518:184–194. https://doi.org/10.1016/j.virol.2018.02.018.
51. Ros C, Bayat N, Wolfisberg R, Almendral JM. 2017. Protoparvovirus cell entry. Viruses 9:313. https://doi.org/10.3390/v9110313.
52. Sánchez-Martínez C, Grueso E, Carroll M, Rommelaere J, Almendral JM. 2012. Essential role of the unordered VP2 N-terminal domain of the parvovirus MVM capsid in nuclear assembly and endosomal enlargement of the virion fivefold channel for cell entry. Virology 432:45–56. https://doi.org/10.1016/j.virol.2012.05.025.
53. Agbandje-McKenna M, Llamas-Saiz AL, Wang F, Tattersall P, Rossmann MG. 1998. Functional implications of the structure of the murine parvovirus, minute virus of mice. Structure 6:1369–1381. https://doi.org/10.1016/S0969-2126(98)00137-3.
54. Kontou M, Govindasamy L, Nam HJ, Bryant N, Llamas-Saiz AL, Foces-Foces C, Hernando E, Rubio MP, McKenna R, Almendral JM, Agbandje-McKenna M. 2005. Structural determinants of tissue tropism and in vivo pathogenicity for the parvovirus minute virus of mice. J Virol 79:10931–10943. https://doi.org/10.1128/JVI.79.17.10931-10943.2005.
55. Tsao J, Chapman MS, Agbandje M, Keller W, Smith K, Wu H, Luo M, Smith TJ, Rossmann MG, Compans RW, Parrish CR. 1991. The three-dimensional structure of canine parvovirus and its functional implications. Science 251:1456–1464. https://doi.org/10.1126/science.2006420.
56. Xie Q, Bu W, Bhatia S, Hare J, Somasundaram T, Azzi A, Chapman MS. 2002. The atomic structure of adeno-associated virus (AAV-2), a vector for human gene therapy. Proc Natl Acad Sci U S A 99:10405–10410. https://doi.org/10.1073/pnas.162250899.
57. Gurda BL, Parent KN, Bladek H, Sinkovits RS, DiMattia MA, Rence C, Castro A, McKenna R, Olson N, Brown K, Baker TS, Agbandje-McKenna M.

2010. Human bocavirus capsid structure: insights into the structural repertoire of the parvoviridae. J Virol 84:5880–5889. https://doi.org/10.1128/JVI.02719-09.
58. Kaufmann B, Lopez-Bueno A, Mateu MG, Chipman PR, Nelson CD, Parrish CR, Almendral JM, Rossmann MG. 2007. Minute virus of mice, a parvovirus, in complex with the Fab fragment of a neutralizing monoclonal antibody. J Virol 81:9851–9858. https://doi.org/10.1128/JVI.00775-07.
59. Lopez-Bueno A, Mateu MG, Almendral JM. 2003. High mutant frequency in populations of a DNA virus allows evasion from antibody therapy in an immunodeficient host. J Virol 77:2701–2708. https://doi.org/10.1128/JVI.77.4.2701-2708.2003.
60. Gardiner EM, Tattersall P. 1988. Mapping of the fibrotropic and lymphotropic host range determinants of the parvovirus minute virus of mice. J Virol 62:2605–2613.
61. Lopez-Bueno A, Rubio MP, Bryant N, McKenna R, Agbandje-McKenna M, Almendral JM. 2006. Host-selected amino acid changes at the sialic acid binding pocket of the parvovirus capsid modulate cell binding affinity and determine virulence. J Virol 80:1563–1573. https://doi.org/10.1128/JVI.80.3.1563-1573.2006.
62. Lopez-Bueno A, Segovia JC, Bueren JA, O'Sullivan MG, Wang F, Tattersall P, Almendral JM. 2008. Evolution to pathogenicity of the parvovirus minute virus of mice in immunodeficient mice involves genetic heterogeneity at the capsid domain that determines tropism. J Virol 82:1195–1203. https://doi.org/10.1128/JVI.01692-07.
63. Merchlinsky MJ, Tattersall PJ, Leary JJ, Cotmore SF, Gardiner EM, Ward DC. 1983. Construction of an infectious molecular clone of the autonomous parvovirus minute virus of mice. J Virol 47:227–232.
64. Tullis GE, Burger LR, Pintel DJ. 1993. The minor capsid protein VP1 of the autonomous parvovirus minute virus of mice is dispensable for encapsidation of progeny single-stranded DNA but is required for infectivity. J Virol 67:131–141.
65. Gil-Ranedo J, Hernando E, Riolobos L, Domínguez C, Kann M, Almendral JM. 2015. The mammalian cell cycle regulates parvovirus nuclear capsid assembly. PLoS Pathog 11:e1004920. https://doi.org/10.1371/journal.ppat.1004920.
66. Riolobos L, Reguera J, Mateu MG, Almendral JM. 2006. Nuclear transport of trimeric assembly intermediates exerts a morphogenetic control on the icosahedral parvovirus capsid. J Mol Biol 357:1026–1038. https://doi.org/10.1016/j.jmb.2006.01.019.
67. Lombardo E, Ramirez JC, Agbandje-McKenna M, Almendral JM. 2000. A beta-stranded motif drives capsid protein oligomers of the parvovirus minute virus of mice into the nucleus for viral assembly. J Virol 74:3804–3814. https://doi.org/10.1128/JVI.74.8.3804-3814.2000.
68. Almendral JM. 2013. Assembly of simple icosahedral viruses. Subcell Biochem 68:307–328. https://doi.org/10.1007/978-94-007-6552-8_10.
69. Pillet S, Annan Z, Fichelson S, Morinet F. 2003. Identification of a nonconventional motif necessary for the nuclear import of the human parvovirus B19 major capsid protein (VP2). Virology 306:25–32. https://doi.org/10.1016/S0042-6822(02)00047-8.
70. Boisvert M, Bouchard-Lévesque V, Fernandes S, Tijssen P. 2014. Classic nuclear localization signals and a novel nuclear localization motif are required for nuclear transport of porcine parvovirus capsid proteins. J Virol 88:11748–11759. https://doi.org/10.1128/JVI.01717-14.
71. Giordano RJ, Anobom CD, Cardó-Vila M, Kalil J, Valente AP, Pasqualini R, Almeida FC, Arap W. 2005. Structural basis for the interaction of a vascular endothelial growth factor mimic peptide motif and its corresponding receptors. Chem Biol 12:1075–1083. https://doi.org/10.1016/j.chembiol.2005.07.008.
72. Starzec A, Ladam P, Vassy R, Badache S, Bouchemal N, Navaza A, Du Penhoat CH, Perret GY. 2007. Structure-function analysis of the antiangiogenic ATWLPPR peptide inhibiting VEGF (165) binding to neuropilin-1 and molecular dynamics simulations of the ATWLPPR/neuropilin-1 complex. Peptides 28:2397–2402. https://doi.org/10.1016/j.peptides.2007.09.013.
73. Louis Jeune V, Joergensen JA, Hajjar RJ, Weber T. 2013. Pre-existing anti-adeno-associated virus antibodies as a challenge in AAV gene therapy. Hum Gene Ther Methods 24:59–67. https://doi.org/10.1089/hgtb.2012.243.
74. Lang SI, Giese NA, Rommelaere J, Dinsart C, Cornelis JJ. 2006. Humoral immune responses against minute virus of mice vectors. J Gene Med 8:1141–1150. https://doi.org/10.1002/jgm.940.
75. Langeveld JP, Casal JI, Vela C, Dalsgaard K, Smale SH, Puijk WC, Meloen RH. 1993. B-cell epitopes of canine parvovirus: distribution on the primary structure and exposure on the viral surface. J Virol 67:765–772.
76. Bloom ME, Best SM, Hayes SF, Wells RD, Wolfinbarger JB, McKenna R, Agbandje-McKenna M. 2001. Identification of Aleutian mink disease parvovirus capsid sequences mediating antibody-dependent enhancement of infection, virus neutralization, and immune complex formation. J Virol 75:11116–11127. https://doi.org/10.1128/JVI.75.22.11116-11127.2001.
77. Hafenstein S, Bowman VD, Sun T, Nelson CD, Palermo LM, Chipman PR, Battisti AJ, Parrish CR, Rossmann MG. 2009. Structural comparison of different antibodies interacting with parvovirus capsids. J Virol 83:5556–5566. https://doi.org/10.1128/JVI.02532-08.
78. Gurda BL, DiMattia MA, Miller EB, Bennett A, McKenna R, Weichert WS, Nelson CD, Chen W-J, Muzyczka N, Olson NH, Sinkovits RS, Chiorini JA, Zolotutkhin S, Kozyreva OG, Samulski RJ, Baker TS, Parrish CR, Agbandje-McKenna M. 2013. Capsid antibodies to different adeno-associated virus serotypes bind common regions. J Virol 87:9111–9124. https://doi.org/10.1128/JVI.00622-13.
79. Tseng YS, Agbandje-McKenna M. 2014. Mapping the AAV capsid host antibody response toward the development of second generation gene delivery vectors. Front Immunol 5:9. https://doi.org/10.3389/fimmu.2014.00009.
80. Tse LV, Klinc KA, Madigan VJ, Castellanos Rivera RM, Wells LF, Havlik LP, Smith JK, Agbandje-McKenna M, Asokan A. 2017. Structure-guided evolution of antigenically distinct adeno-associated virus variants for immune evasion. Proc Natl Acad Sci U S A 114:E4812–E4821. https://doi.org/10.1073/pnas.1704766114.
81. Lopez-Bueno A, Valle N, Gallego JM, Perez J, Almendral JM. 2004. Enhanced cytoplasmic sequestration of the nuclear export receptor CRM1 by NS2 mutations developed in the host regulates parvovirus fitness. J Virol 78:10674–10684. https://doi.org/10.1128/JVI.78.19.10674-10684.2004.
82. Rubio MP, Lopez-Bueno A, Almendral JM. 2005. Virulent variants emerging in mice infected with the apathogenic prototype strain of the parvovirus minute virus of mice exhibit a capsid with low avidity for a primary receptor. J Virol 79:11280–11290. https://doi.org/10.1128/JVI.79.17.11280-11290.2005.
83. Shein HM, Enders JF, Levinthal JD. 1962. Transformation induced by simian virus 40 in human renal cell cultures. II. Cell-virus relationships. Proc Natl Acad Sci U S A 48:1350–1357. https://doi.org/10.1073/pnas.48.8.1350.
84. Lombardo E, Ramirez JC, Garcia J, Almendral JM. 2002. Complementary roles of multiple nuclear targeting signals in the capsid proteins of the parvovirus minute virus of mice during assembly and onset of infection. J Virol 76:7049–7059. https://doi.org/10.1128/JVI.76.14.7049-7059.2002.
85. Maroto B, Ramirez JC, Almendral JM. 2000. Phosphorylation status of the parvovirus minute virus of mice particle: mapping and biological relevance of the major phosphorylation sites. J Virol 74:10892–10902. https://doi.org/10.1128/JVI.74.23.10892-10902.2000.
86. Hernando E, Llamas-Saiz AL, Foces-Foces C, McKenna R, Portman I, Agbandje-McKenna M, Almendral JM. 2000. Biochemical and physical characterization of parvovirus minute virus of mice virus-like particles. Virology 267:299–309. https://doi.org/10.1006/viro.1999.0123.
87. Ramirez JC, Santaren JF, Almendral JM. 1995. Transcriptional inhibition of the parvovirus minute virus of mice by constitutive expression of an antisense RNA targeted against the NS-1 transactivator protein. Virology 206:57–68. https://doi.org/10.1016/S0042-6822(95)80019-0.
88. Boissy R, Astell CR. 1985. An Escherichia coli recBCsbcBrecF host permits the deletion-resistant propagation of plasmid clones containing the 5′-terminal palindrome of minute virus of mice. Gene 35:179–185. https://doi.org/10.1016/0378-1119(85)90170-2.
89. Santaren JF, Ramirez JC, Almendral JM. 1993. Protein species of the parvovirus minute virus of mice strain MVMp: involvement of phosphorylated VP-2 subtypes in viral morphogenesis. J Virol 67:5126–5138.